FORMOSAT-3/COSMIC GPS Radio Occultation Mission: Preliminary Results

Yuei-An Liou, *Senior Member, IEEE*, Alexander G. Pavelyev, Shuo-Fang Liu, Alexey A. Pavelyev, Nick Yen, C.-Y. Huang, and Chen-Joe Fong, *Student Member, IEEE*

***Abstract*—The Formosa Satellite-3 and Constellation Observing System for the Meteorology, Ionosphere, and Climate (FORMOSAT-3/COSMIC) radio occultation (RO) mission has been successfully launched on April 14, 2006. The FORMOSAT-3/COSMIC mission uses global positioning system (GPS) signals to study the atmosphere and the ionosphere with global coverage. Receivers that are installed onboard of the six small FORMOSAT-3/COSMIC satellites register the phase and the amplitude of radio waves at two GPS frequencies. We give a preliminary analysis of the first RO measurements that are provided by the FORMOSAT-3/COSMIC mission. The geographical distribution of the first FORMOSAT-3/COSMIC RO experiments is shown. We demonstrate that the performance of the first measurements allows obtaining the vertical profiles of the refractivity, temperature, and pressure for the considered FORMOSAT-3/COSMIC RO events with expected accuracy, which is quite similar to the accuracy of the previous Challenging Mini-Satellite Payload and Gravity Recovery and Climate Experiment RO missions. New elements in the RO technology are suggested for further improving the accuracy and broadening the application range of the RO method. We emphasize new directions in applying the RO method to measure the vertical gradients of the refractivity in the atmosphere, to determine the temperature regime in the upper stratosphere, and to investigate the internal wave activity in the atmosphere. We find a significant correlation between the phase acceleration and the intensity variations in the RO signals that are emitted by GPS satellites and registered by the FORMOSAT-3/COSMIC satellites. This correlation opens a way to locate the layered structures in the propagation medium based on simultaneous observations of the radio wave intensity and the phase variations in trans-ionospheric satellite-to-satellite links.**

***Index Terms*—Atmospheric refractivity, global positioning system (GPS) remote sensing, layered structures.**

Manuscript received October 5, 2006; revised April 18, 2007. This work was supported in part by the Russian Foundation for Basic Researches under Grant 06-02-17071 and in part by the National Science Council of Taiwan (NSC) under Grant NSC 94-2811-M-008-055.

Y.-A. Liou is with the Center for Space and Remote Sensing Research, National Central University, Taoyuan 32001, Taiwan, R.O.C., with the College of Electrical Engineering and Computer Science, Ching Yun University, Chungli 320, Taiwan, R.O.C., and also with the National Space Organization, Hsinchu 30050, Taiwan, R.O.C. (e-mail: yueian@csrsr.ncu.edu.tw).

A. G. Pavelyev and A. A. Pavelyev are with the Institute of Radio Engineering and Electronics, Russian Academy of Sciences, Fryazino, 141190 Moscow Region, Russia (e-mail: pvlv@ms.ire.rssi.ru).

S.-F. Liu is with the Department of Industrial Design, National Cheng Kung University, Tainan 701, Taiwan, R.O.C. (e-mail: liusf@mail.ncku.edu.tw).

N. Yen, C.-Y. Huang, and C.-J. Fong are with the National Space Organization, Hsinchu 300, Taiwan, R.O.C. (e-mail: longine@nspo.org.tw).

Digital Object Identifier 10.1109/TGRS.2007.903365

I. Introduction

THE MAIN idea of the radio occultation (RO) technique has been suggested in 1964 [1]. Since 1975, the RO method has been applied to the study of the Earth's atmosphere and ionosphere using communication satellites [2]. The preliminary RO experiments, from 1975 to 1995, verified the methodology of the RO measurements and demonstrated its great promise for the study of the Earth's atmosphere and ionosphere on a global scale. Applying the RO method to the systematic monitoring of the Earth's atmosphere using global positioning system (GPS) signals has been proposed in 1988–1990 [3], [4] and was demonstrated with the low Earth orbiting (LEO) satellite MicroLab-1 [GPS/Meteorology (GPS/MET) mission], which was launched on April 3, 1995 [5], [6]. Vertical profiles of the ray bending angle and refractivity were retrieved from the raw MicroLab-1 observations, which, in turn, were used to compute the ionospheric electron density and neutral atmospheric density, pressure, geopotential heights of constant pressure levels, temperature, and moisture vertical profiles [5]–[10]. In addition, reflected signals from the ocean surface are used to measure sea surface roughness, delay/Doppler mapping, and wind estimate [11], [12]. Since then, several GPS RO missions have been launched, which include ØRSTED, Stellenbosch University Satellite (SUNSAT), Challenging Mini-Satellite Payload (CHAMP), Satelite de Aplicaciones Cientificas-C (SAC-C), and Gravity Recovery and Climate Experiment (GRACE) [13]–[19]. Today, the database of the GPS/MET, CHAMP, and SAC-C RO missions covers about ten years of observations, which enable the study of seasonal and geographical dependencies of atmospheric and ionospheric phenomena on a global scale [5], [17], [20]–[24]. Now, the RO data are used for validation analyses of atmospheric profiles produced by different space-based remote-sensing missions, e.g., verification of the retrieved atmospheric profiles from the Earth Observing System Microwave Limb Sounder instrument on the Aura satellite [25]. New refinements on the RO technique have been considered, which include the following: 1) atmospheric gravity waves (GWs) morphology [20], [24], [26]–[31]; 2) retrievals of the refractivity by use of the amplitude data [31]–[34]; and 3) estimating parameters and locating wave structures in the ionosphere [35]–[38] and in the atmosphere [24].

In this paper, we briefly discuss the modernizations of the RO method and describe their application to the first Formosa Satellite-3 and Constellation Observing System for Meteorology, Ionosphere, and Climate (FORMOSAT-3/COSMIC)

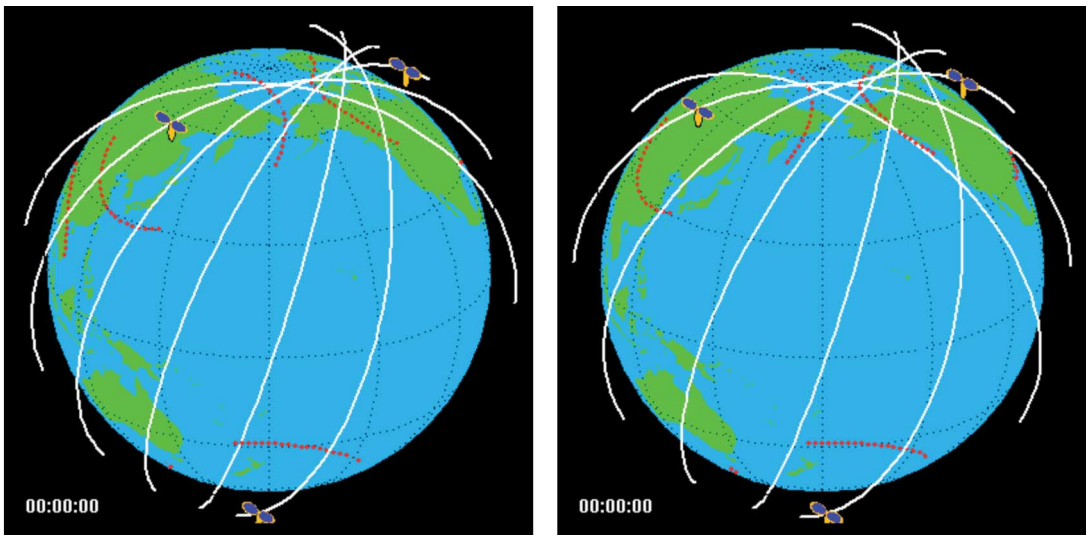

Fig. 1. Comparison of constellations with 24° and 30° separation between adjoining planes. The 24° orbit separation will provide nonuniform occultation coverage in local solar time. It is not favorable for ionospheric monitoring and for studying climate seasonal variability. Uniform coverage is extremely important for a wide class of studies. The coverage of constellation with 30° separation is better than that with 24° separation.

experiments. In Section II, the constellation and deployment of the FORMOSAT-3/COSMIC satellites are introduced. In Section III, the equations that describe the basic relationships of the RO technique are presented, and a new connection between the phase acceleration and the refraction attenuation is established. In Section IV, preliminary results of the FORMOSAT-3/COSMIC mission are analyzed. In Section V, the joint analysis of the phase and amplitude data is provided for measuring the horizontal wind perturbations and energy associated with the atmospheric internal waves.

II. Status of the FORMOSAT-3/COSMIC Mission

Termed as the FORMOSAT-3/COSMIC mission, the new constellation's primary science goal is to obtain in near real time the vertical profiles of temperature, pressure, refractivity, and water vapor in the neutral atmosphere and electron density in the ionosphere with global coverage at different altitudes. The measurements during five years of mission existence will provide about 2500 soundings per day, thus generating an extensive body of information to support operational global weather prediction, climate change monitoring, ionospheric phenomena, space weather research, and estimations of connections of meteorological and ionospheric processes with solar activity and human impact.

The six small FORMOSAT-3 satellites that were delivered by one U.S. Minotaur launch vehicle into space on April 14, 2006 opened new possibilities for systematic mass scale RO studies of the Earth atmosphere and ionosphere at different altitudes and in various geographical and seasonal conditions. The Minotaur launch vehicle placed the six FORMOSAT-3 satellites into a circular parking orbit with the following altitude and inclination: perigee altitude at 492 km, apogee altitude at 538 km, and inclination at 71.99°. The mission configuration of the FORMOSAT-3 satellites has been changed from the initial 24° to 30° separation between adjacent orbit planes

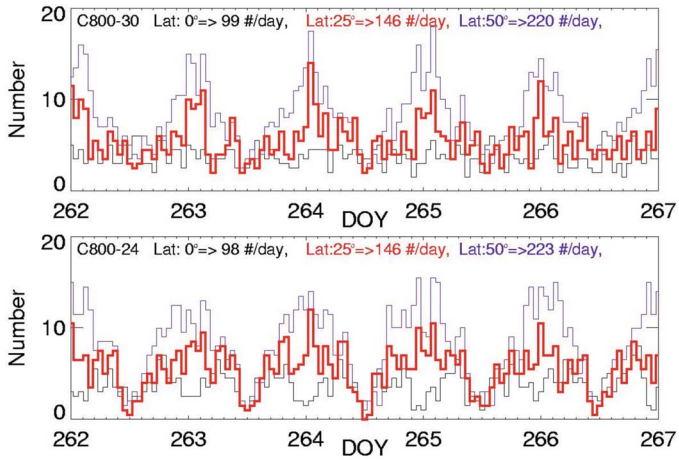

Fig. 2. Number of RO events at different latitudes versus time. The number of RO events is calculated at longitude equal to 120° and latitudes equal to 0°, 25°, and 50°. The 30° constellation shows better distribution versus time.

to achieve better uniformity in global coverage, as shown in Figs. 1 and 2. The initial scheme for the constellation with 24° separation between adjacent orbit planes has envisaged a shorter duration for satellites deployment at the 800-km mission orbit with the single purpose of beginning sooner the basic science investigations. Surprisingly, the extensive volume of the RO data as collected at the current orbits during permanent constellation deployment was found to be sufficient for the user's community.

The total numbers of RO events as collected and processed up to February 2007 are shown in Fig. 3. As seen in Fig. 3, the daily number of the useful RO events increased from 200–400 in July 2006 up to 1300–1500 in January 2007. In February 2007, the FORMOSAT-3/COSMIC mission daily processed ∼1500 good atmospheric soundings, which is above the number of worldwide radiosondes launched per day. In the

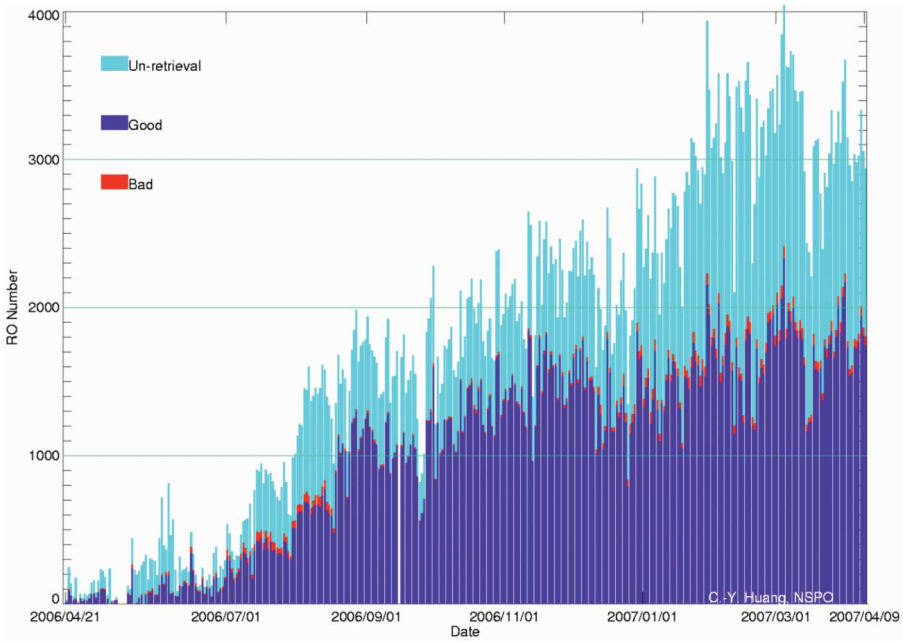

Fig. 3. Daily number of RO events processed up to April 2007. Aqua color bars are daily number of RO events observed by FORMOSAT-3. Blue bars are daily number of retrieved vertical atmospheric profiles, and red color bars are bad profiles.

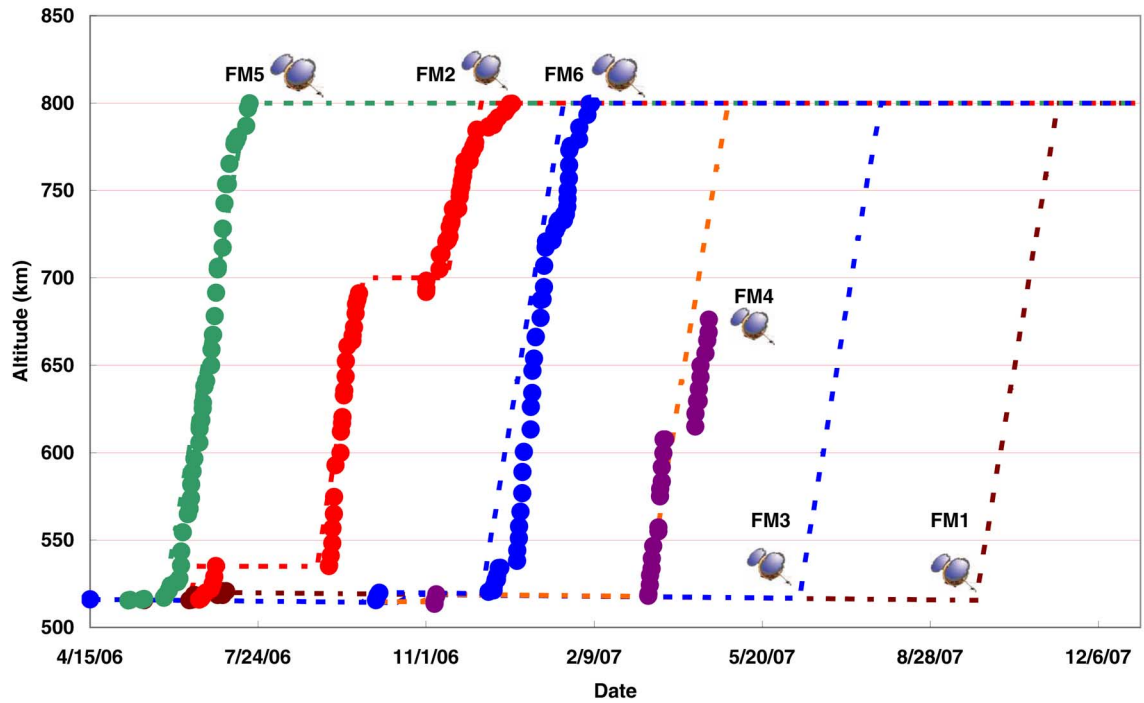

Fig. 4. FORMOSAT-3 constellation deployment profile versus time. The FORMOSAT-3 satellites flight model no. 2 (FM2), no. 5 (FM5), and no. 6 (FM6) have arrived to the 800-km orbit in early February 2007. The final mission constellation configuration will arrive to the 800-km orbit around November 30, 2007.

current state of the constellation, the FORMOSAT-3/COSMIC mission daily provides much more profiles as ever before. Therefore, the period for the constellation deployment phase has been prolonged from 13 to 20 months by changing the orbit planes separation to 30°. The constellation deployment profile and the constellation configuration that corresponds to April 2007 are shown in Figs. 4 and 5, respectively. In the beginning of the constellation deployment, the FORMOSAT-3 satellite FM5 was the first spacecraft being maneuvered into the 800-km orbit altitude. The orbit plane of the FM5 satellite is used now as the Right Ascension of Ascending Node (RAAN) reference plane for the other FORMOSAT-3 satellites to drift their orbit planes into the proper RAAN phase. The FORMOSAT-3 satellites FM2 and FM6 have arrived to the 800-km mission

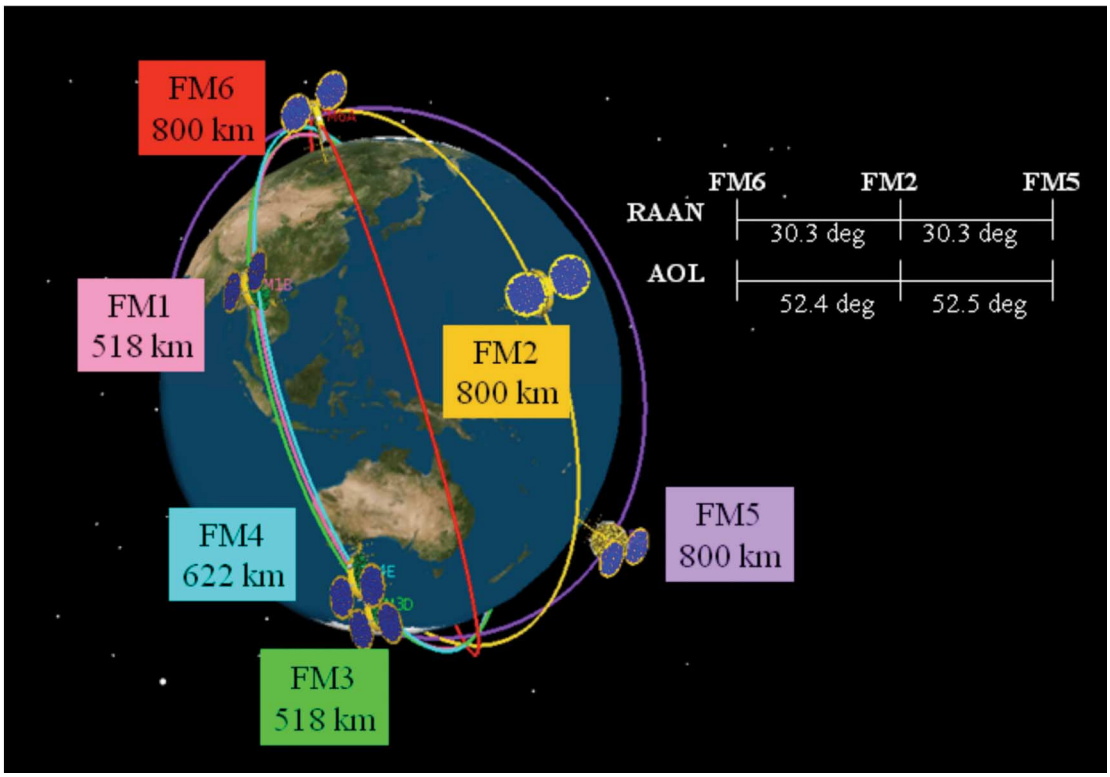

Fig. 5. FORMOSAT-3 constellation configuration in April 2007. The FORMOSAT-3 satellite flight model no. 2 (FM2), no. 5 (FM5), and no. 6 (FM6) are already installed at their working orbits with 800-km height. The FORMOSAT-3 satellites flight model no. 1 (FM1) and no. 3 (FM3) up to now are on the intermediate orbits with 518-km height, and no. 4 (FM4) is performed with thrusting burns as of the writing of this paper in April 2007.

orbit (Figs. 4 and 5) in February 2007. The optimized constellation configuration with six orbit planes separated by 30° at the 800-km altitude will be finally developed around November 30, 2007.

III. RO Method

The key geometric parameters of a GPS RO experiment are shown in Fig. 6. Point O denotes the global spherical symmetry's center of the Earth's atmosphere and ionosphere. Radio waves emitted by the GPS satellite (point G) are detected by the receiver onboard the LEO satellite (point L) after their propagation along ray GTL, where T is the ray perigee. At point T, the ray's distance from the Earth's surface h is minimal, and the gradient of refractivity $N(h)$ is perpendicular to the ray trajectory GTL (Fig. 6). The projection of point T on the Earth's surface determines the geographical coordinates of the RO region. The records of the RO signal along the LEO trajectory at two GPS frequencies $f_1 = 1575.42$ MHz and $f_2 = 1227.6$ MHz are the radio holograms, which contain the amplitudes $A_1(t)$ and $A_2(t)$, respectively, along the phase path excesses $\Phi_1(t)$ and $\Phi_2(t)$ of the radio field as functions of time. The vertical velocity of the occultation beam path $v_\perp$ is about 2 km/s. This $v_\perp$ value is many times greater than the ones that correspond to the motion of layers in the ionosphere and the atmosphere. Therefore, the satellite radio holograms contain quasi-instantaneous image of the Earth environment in the RO region. The phase variations of the RO signal can be applied to determine the impact parameter p of the ray

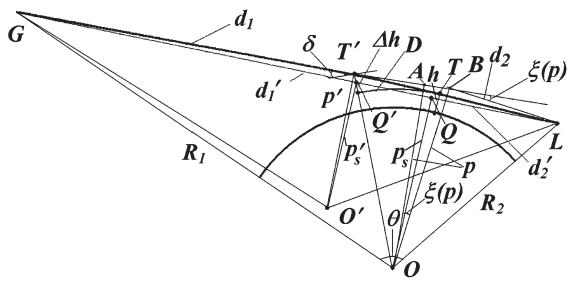

Fig. 6. Ray path configuration in a spherically symmetric media during the RO experiment. The vertical gradient of the refractivity is perpendicular to the radio ray GTL in the tangent point T. In the case of the spherical symmetric atmosphere with center of symmetry in point O, the tangent point T coincides with the radio ray perigee. The center of spherical symmetry O and the tangent point T can be displaced owing to the horizontal gradients in the atmosphere to point O' and T', respectively.

trajectory GTL and the bending angle $\xi(p)$ (Fig. 6) by use of known satellite trajectory data [22]. Then, the electron density $N_e(p)$ in the ionosphere and the vertical profiles of refractivity $N(p)$ in the neutral atmosphere can be determined by different methods based on the Abel transform [33], [34], [39]–[41]. The altitude h can be determined from the known values of the Earth curvature radius a_e, impact parameter p, and refractivity $N(p)$ under the assumption of spherical symmetry with the center at point O [22]. The amplitude variations of the RO signals are also used to determine the vertical gradient of the refractivity $dN(h)/dh$ and electron density $dN_e(h)/dh$ [42]. Note that at GPS frequencies, the refractivity is small, and the

location of the point T in the upper atmosphere and ionosphere practically coincides with the projection of the center of spherical symmetry O on the line-of-sight direction GL—point Q (Fig. 6). Therefore, the height h of the ray perigee T can be directly calculated by use of a known location of the spherical symmetry center O and trajectory data. Below, we will consider the basic relationships of the RO method with the addition of the important connection between the phase acceleration and the refraction attenuation of radio waves.

There is the significant connection between the phase path excess $\Phi(t)$ and the amplitude $A(t)$ of radio holograms considered as functions of time at two GPS frequencies f_1 and f_2. This connection is described for the case of local spherical symmetry by equations previously found in [24], [31], [43], and [44], i.e.,

$$\Phi(p) = L(p) + \kappa(p) - R_0 \tag{1}$$

$$X(p) = pR_0^2[R_1R_2d_1d_2\sin\theta\,|\partial\theta/\partial p|]^{-1} \tag{2}$$

$$\partial\theta/\partial p = d\xi/dp - (1/d_1 + 1/d_2) \tag{3}$$

$$L(p) = \left(R_1^2 - p^2\right)^{1/2} + \left(R_2^2 - p^2\right)^{1/2} + p\xi(p)$$

$$R_0 = \left(R_1^2 - p_s^2\right)^{1/2} + \left(R_2^2 - p_s^2\right)^{1/2} \tag{4}$$

$$d_1 = \left(R_1^2 - p^2\right)^{1/2} \quad d_2 = \left(R_2^2 - p^2\right)^{1/2} \tag{5}$$

where $\kappa(p)$ is the main refractivity part of the phase path excess, $\xi(p) = -d\kappa(p)/dp$ is the refraction angle, $\theta(p)$ is the central angle, p and p_s are the impact parameters of the ray trajectory GTL and the line-of-sight GQL, respectively, R_0, R_1, and R_2 are the distances GL, OG, and OL, respectively, $L(p)$ is the distance $GABL$, and d_1 and d_2 are two short lengths, i.e., GA and BL, which are approximately equal to GQ and QL (Fig. 6). The refraction angle $\xi(p)$ is connected with the central angle θ (Fig. 6), i.e.,

$$\theta = \pi + \xi(p) - \sin^{-1}(p/R_1) - \sin^{-1}(p/R_2)$$

$$\theta = \pi - \sin^{-1}(p_s/R_1) - \sin^{-1}(p_s/R_2) \tag{6}$$

$$\xi(p) = \sin^{-1}(p/R_1) + \sin^{-1}(p/R_2) - \sin^{-1}(p_s/R_1) - \sin^{-1}(p_s/R_2). \tag{7}$$

Two different expressions (6) for the central angle θ can be used to obtain the connection (7) between the impact parameters p_s and p and the refraction angle $\xi(p)$. From (1) and (6), one can obtain by differentiation of the phase excess $\Phi(p)$ and the central angle θ on time the relationship that connects the Doppler frequency of the RO signal with the impact parameters p and p_s, i.e.,

$$d\Phi(p)/dt = (p - p_s)d\theta/dt + (d_1 - d_{1s})R_1^{-1}dR_1/dt + (d_2 - d_{2s})R_2^{-1}dR_2/dt \tag{8}$$

$$d\theta/dt = \partial\theta/\partial p_s dp_s/dt - p_s \times \left[(d_{1s}R_1)^{-1}dR_1/dt + (d_{2s}R_2)^{-1}dR_2/dt\right]$$

$$d_{1s} = \left(R_1^2 - p_s^2\right)^{1/2} \quad d_{2s} = \left(R_2^2 - p_s^2\right)^{1/2} \tag{9}$$

where d_{1s} and d_{2s} are the distances GQ and QL, respectively (Fig. 6). After substitution of (9) in (8), one can obtain

$$d\Phi(p)/dt = -(p - p_s) \times \Big\{(1/d_{1s} + 1/d_{2s})dp_s/dt + \left(p^2 - p_s^2\right) \times \Big\{R_1dR_1/dt\,[d_{1s}(d_{1s} + d_1)(pd_{1s} + p_sd_1)]^{-1} + R_2dR_2/dt\,[d_{2s}(d_{2s} + d_2) \times (pd_{2s} + p_sd_2)]^{-1}\Big\}\Big\}. \tag{10}$$

Equations (6)–(10) are valid for the general case of the noncircular orbits of the GPS and LEO satellites. Equation (10) can be simplified under the condition

$$|1/d_{1s} + 1/d_{2s})dp_s/dt| \gg \Big|\left(p^2 - p_s^2\right)\Big\{R_1dR_1/dt\,[d_{1s}(d_{1s} + d_1)(pd_{1s} + p_sd_1)]^{-1} + R_2dR_2/dt\,[d_{2s}(d_{2s} + d_2)(pd_{2s} + p_sd_2)]^{-1}\Big\}\Big| \tag{11}$$

which is valid if $|(p - p_s)dR_{1,2}/dt| \ll p_s|dp_s/dt|$. This inequality is valid for all practical RO situations. Under an indicated approximation, one can obtain from (10) a formula for the estimation of the difference $p - p_s$ on the Doppler frequency $d\Phi(p)/dt$, i.e.,

$$d\Phi(p)/dt = -(p - p_s)(1/d_{1s} + 1/d_{2s})dp_s/dt. \tag{12}$$

The values p_s, dp_s/dt, d_{1s}, and d_{2s} can be delivered from the orbital data, and the phase delays $\Phi_{1,2}(p)$ are the objects of measurements and are given in the phase parts of radio holograms at frequencies f_1 and f_2. Therefore, one may obtain (after the ionospheric correction) the dependence of the refraction angle ξ on the impact parameter p and then, by use of Abel inversion, retrieve the vertical profiles of the refractivity $N(h)$, pressure $P(h)$, temperature $T(h)$, humidity $e(h)$, and electron density in the ionosphere $N_e(h)$ [22].

Below, we will consider the new relationship that connects the phase acceleration and the refraction attenuation of radio waves. Under conditions

$$|p - p_s| \ll p_s \tag{13}$$

$$|(p - p_s)d(\partial\theta/\partial p_s)/dt| \ll |(dp/dt - dp_s/dt)\cdot\partial\theta/\partial p_s| \tag{14}$$

by use of $dp/dt - dp_s/dt \approx [X(t) - 1]dp_s/dt$ [24], one can obtain from (12)

$$1 - X(t) = ma \quad a = d^2\Phi(t)/dt^2 \tag{15}$$

$$m = q/(dp_s/dt)^2 \tag{16}$$

$$q = d_1d_2/(d_1 + d_2) \quad d_1 + d_2 = R_0. \tag{17}$$

Equation (15) indicates the equivalence between the variations of the phase path excess acceleration $a = d^2\Phi(t)/dt^2$ and

the refraction attenuation $X(t)$, which may be verified by use of the RO data. Usually, during the RO experiments, parameters m and dp_s/dt are known from the orbital data because the location of the spherical symmetry center O and its projection on the line-of-sight point Q are known, and the distance GT d_1 and TL d_2 can be easily estimated as $d_{1,2} = (R_{1,2}^2 - p^2)^{1/2}$ (Fig. 6). Therefore, (15) gives a possibility to recalculate the phase acceleration a to the refraction attenuation X_a. This is useful for excluding the systematic errors from the phase and/or amplitude data and also for the estimation of the absorption in the atmosphere. The refraction attenuation X_a is determined from the amplitude data as a ratio of the intensity of the radio signal that propagates through the atmosphere $I_a(t)$ to its intensity in free space I_s, i.e.,

$$X_a(t) = I_a(t)/I_s. \tag{18}$$

Thus, the experimental value X_a is the sum of the refractive and absorption contributions. However, the phase acceleration depends on the refraction effect only. This gives a possibility to determine the absorption in the atmosphere $Y(t)$ as a ratio

$$Y(t) = X_a(t)/(1 - ma). \tag{19}$$

This possibility must be investigated in detail because in the future satellite RO mission, the measurement of the absorption effects due to water vapor and minor atmospheric gas constituents is planned, and the difficulties will consist of removing the refraction attenuation effect from the amplitude data. Equation (19) indicates the feasible way to solve this problem. Moreover, relationship (19) may be useful for estimating the conditions for communication in the Ku/K bands between two LEO satellites in a RO geometry [45]. However, the detailed analysis of the methodology is beyond the scope of this paper and will be considered in future publications.

At the GPS frequencies, the absorption effect in RO experiment mainly caused by the atmospheric oxygen is about 2–3 dB in the lower troposphere and is small in the upper troposphere and the stratosphere. Therefore, (15)–(17) are useful in controlling the deflections from the spherical symmetry by use of a joint analysis of the amplitude and phase variations in the RO signal.

The horizontal gradients in the ionosphere and the atmosphere can displace the tangent point T along the ray trajectory to point T' because of the deflection of the center of the spherical symmetry from its standard position—point O to point O' (Fig. 6). As a consequence, the value of the distance $T'L$ [approximately equal to LQ' (Fig. 6)] will change to d_2', and the parameter m will also change its magnitude. However, (15)–(17) are valid in the case of local spherical symmetry with the new center O'. Therefore, if the magnitude of the parameter m will be estimated from the experimental data, then it is possible to find the new value of distance $T'L$ d_2' and, thus, determine the location of the new tangent point T' relative to the point T (or L). For the determination of the parameter m from the experimental data, we can assume that the value m is a slowly changing function of time. If the noise is very small, the averaging is not necessary, and the parameter m can be determined directly from (15) as a ratio

$$m = [1 - X(t)]/a. \tag{20}$$

In the presence of noise, the value $m(t_\kappa)$ that corresponds to some instant of time t_κ can be determined from the RO data as a ratio of the average of the squared refraction attenuation variation and the phase acceleration variations, i.e.,

$$m(t_k) = \left\{ \sum_{i=k-M}^{i=k+M} [X(t_i) - 1]^2 \Big/ \sum_{ik-M}^{i=k+M} [a(t_i)]^2 \right\}^{1/2} \tag{21}$$

where $2M$ is the number of samples for averaging, and $X(t_i)$ and $a(t_i)$ are the current values of the refraction attenuation and phase acceleration variations at the time instant t_i, respectively. Equation (21) is valid if there is a full correlation between the refraction attenuation and the phase acceleration according to (15). In real conditions, there are different sources of amplitude and phase variations of the RO signal (e.g., turbulence, multipath propagation, etc.) that do not obey (15). However, the amplitude and phase variations that correspond to the layered structures in the atmosphere and the ionosphere must obey relationship (15), and therefore, the parameter m can be determined also from the correlation relationship

$$m(t_k) = \sum_{i=k-M}^{i=k+M} [1 - X(t_i)]\, a(t_i) \Big/ \sum_{i=k-M}^{i=k+M} [a(t_i)]^2 . \tag{22}$$

Relationship (22) describes the parameter m as a correlation coefficient between the refraction attenuation $X(t_i)$ and the phase acceleration $a(t_i)$.

When the parameter m is known with sufficient accuracy, one can estimate the distance D between the tangent points T and T' (Fig. 6) by use of (16) and (17), i.e.,

$$D \approx d_2' - d_2 = d_2' - \left(R_2^2 - p^2\right)^{1/2}. \tag{23}$$

When the influence of turbulence, multipath, and instabilities in transmitter and receiver are important, (20)–(23) give three different values of the parameter m and the distance D. Note that one must account for the velocity of point O' in relations (16) and (17). In the case of the Earth's atmosphere and ionosphere, the velocity of motion of layers and, consequently, the velocity of point O' is small as compared with the orbital velocities of the GPS and LEO satellites.

IV. Preliminary Results of the FORMOSAT-3/COSMIC Mission

The geographical distribution of the first ten-day FORMOSAT-3/COSMIC RO mission events is given in Fig. 7 from April 21 to 30, 2006. The total number of RO events is 812 because the main goal of the preliminary phase consists of checking the software and hardware of the receivers onboard the FORMOSAT-3 satellites. After ending the preliminary phase (about 20 months after the launch), the nominal value of the RO events will achieve about 2500 occultations per

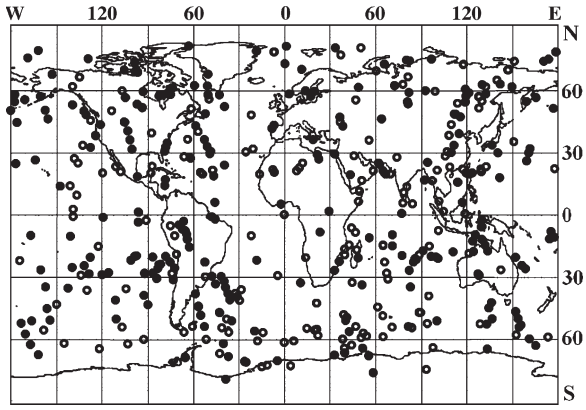

Fig. 7. Geographical distribution of the first ten-day FORMOSAT-3/COSMIC RO events from April 21 to 30, 2006. Open circles correspond to the night events from 2000 to 0800 LT. Closed circles correspond to the day events from 0800 to 2000 LT.

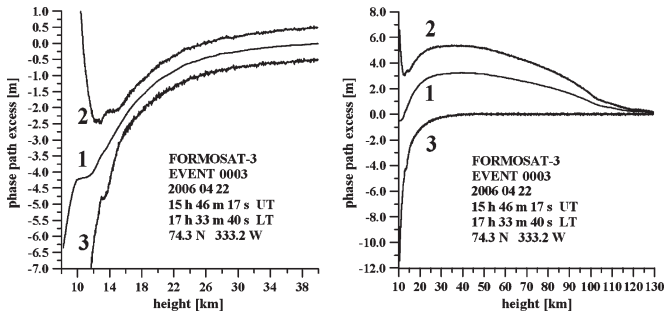

Fig. 8. Phase excesses $\Phi_1(t)$ and $\Phi_2(t)$ (curves 1 and 2) (right panel) before and (left panel) after ionospheric correction. Curve 3 describes the automatically corrected phase delay $\Phi_0(t)$ by use of (24). Curves 2 and 3 are displaced by 0.5 m for better comparison. The noise, which is seen at frequency f_2 (curve 2), is transmitted after linear ionospheric correction to the contribution from the neutral atmosphere (curve 3). The ionospheric correction, which uses the ionospheric model, does not allow the noise transmission to the corrected phase delay at frequency f_1 (curve 1 in the left panel).

day. The near-polar orbit of the FORMOSAT-3 satellite allows global monitoring, which includes monitoring of the North and South Polar Regions and ocean areas. As a rule, the first FORMOSAT-3/COSMIC RO measurements have been provided down to the 5- to 8-km height interval. A tracking firmware for COSMIC receivers has been implemented by Jet Propulsion Laboratory [46]. L1 and L2 signals have been recorded in a closed-loop mode above $\sim$10 km. Below $\sim$10 km, L1 has been recorded in an open-loop mode.

While measuring the neutral atmospheric parameters, the ionospheric correction method is applied to subtract the ionospheric effect from the RO phase data. The linear ionospheric correction of the phase delays is automatically applied in the FORMOSAT-3/COSMIC RO data using the formula [23], [47]

$$\Phi_0(t) = \left[f_1^2\Phi_1(t) - f_2^2\Phi_2(t)\right] / \left(f_1^2 - f_2^2\right) \qquad (24)$$

where $\Phi_0(t)$ is the corrected phase delay, which is included together with the phase delays $\Phi_1(t)$ and $\Phi_2(t)$ in the RO data. The common bending angle correction method [48] requires differentiation of the phase excess on time and, therefore, enlarges the influence of high-frequency noise. The disadvantage of both linear correction methods consists of an increase in the high-frequency noise contribution.

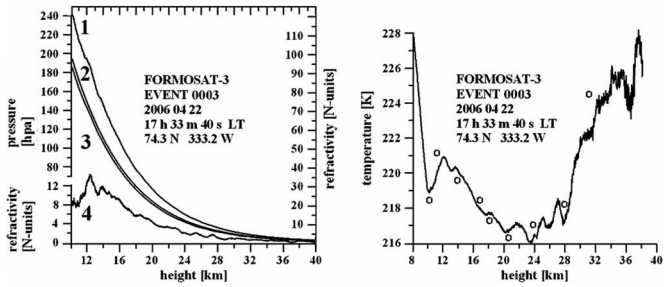

Fig. 9. (Left panel) Results of retrieving the vertical profiles of refractivity $N(h)$ (N units) and pressure $P(h)$ (hPa) from the phase delay $\Phi_1(t)$. The top left vertical axis corresponds to pressure (curve 1), and the bottom left vertical axis is relevant to the refractivity perturbations (curve 4). The right vertical axis corresponds to the vertical profiles of the refractivity calculated by use of standard atmospheric model (curve 2) and the refractivity retrieved from the RO data (curve 3). (Right panel) Results of retrieving the vertical profile of temperature $T(h)$ (K). The data are relevant to the FORMOSAT-3/COSMIC RO event no. 0003 (April 22, 2006, 17 h 33 min 40 s LT), above the western part of the Barents Sea with geographical coordinates 74.3° N, 333.2° W. Open circles indicate the results of NCEP analysis for this area (April 22, 2006, 15 h 00 min UT; http://www.cdc.noaa.gov/cgi-bin) at the altitudes that correspond to pressure 250, 200, 150, 100, 70, 50, 30, 20, and 10 hPa.

To decrease the high-frequency noise contribution, we separately exclude the slow ionospheric trend from both frequencies f_1 and f_2 by use of the ionospheric model IRI-2000. To eliminate a possible bias that the model may introduce into the neutral refractivity profile, we use the reference function, which has been obtained from the phase delay $\Phi_0(t)$ by the least-squares method. Through this method of ionospheric correction, we exclude the ionospheric systematic error in the low-frequency interval and avoid the increase in the high-frequency noise. The suggested method is appropriate during period of minimal solar activity when the ionosphere is quiet. The results of the application of the ionospheric correction to both phase delays f_1 and f_2 and the comparison with linear correction method (24) are shown in Fig. 8. The results shown in Fig. 8 have been obtained after subtracting the phase delays, which are calculated using the model of standard refraction in the atmosphere [43], i.e., $N = N_0 \exp(-H/H_0)$, where H is the height above the Earth surface, N_0 is the refractivity of the atmosphere at $H = 0$, and H_0 is the height scale of the atmosphere. Curves 1–3 in Fig. 8 (right panel) demonstrate the behavior of the phase delays $\Phi_1(t)$ (curve 1), $\Phi_2(t)$ (curve 2), and the linear corrected phase delay $\Phi_0(t)$ (24) as a function of height h in the atmosphere. The noise from frequency $\Phi_2(t)$ is seen also in the phase delay $\Phi_0(t)$ (curve 3). Application of the ionospheric model allows excluding the ionospheric effect from both phase delays $\Phi_1(t)$ (curve 1) and $\Phi_2(t)$ (curve 2) without increasing the noise intensity (Fig. 8, left panel). For better comparison with the results of linear ionospheric correction (curve 3), curves 2 and 3 are displaced by 0.5 m in the opposite sites (Fig. 8, left panel).

The model-dependent ionospheric correction minimizes the noise level in the retrieved atmospheric refractivity. This allows obtaining high accuracy in the vertical profiles of pressure and

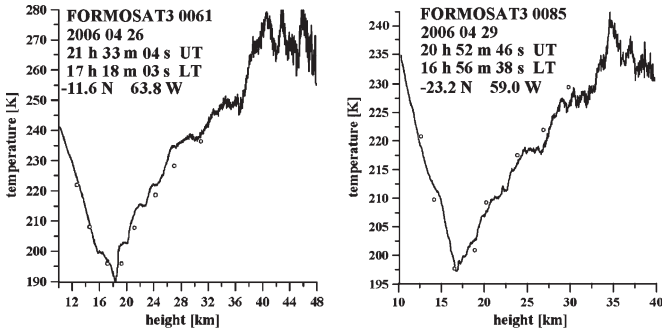

Fig. 10. Comparison of the temperature vertical profiles above (left panel) the equatorial and (right panel) the tropical part of South America.

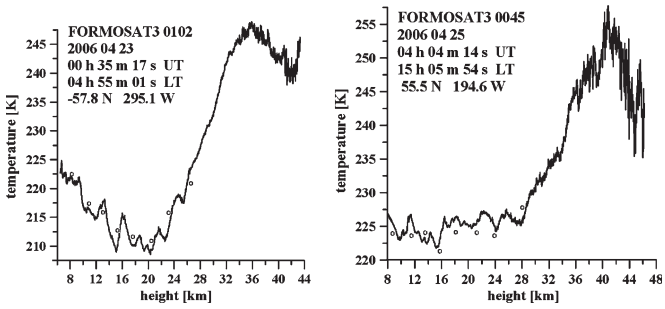

Fig. 11. Comparison of the temperature vertical profiles in the moderate-latitude areas above (left panel) the southern part of the Indian Ocean and (right panel) the northern part of the Pacific Ocean.

temperature over the RO region. The results of retrieving the vertical profiles of refractivity $N(h)$ (N units), pressure $P(h)$ (hPa), and temperature $T(h)$ (K) from the phase delay $\Phi_1(t)$ are demonstrated in Fig. 9 for the FORMOSAT-3/COSMIC RO event 0003 (April 22, 2006, 17 h 33 min 40 s LT, geographical coordinates 74.3° N, 333.2° W). The data, which are shown in Fig. 9 (left panel), are relevant to the vertical profiles of pressure $P(h)$ (curve 1), refractivity $N_m(h)$, which is obtained from the standard model of the atmosphere (curve 2), refractivity $N(h)$, which is retrieved from the phase delay Φ_1 (curve 3), and to the difference $N_m(h) - N(h)$ (curve 4). The retrieved vertical profile of the refractivity is below the standard atmospheric refractivity profile because of the geographical location, i.e., the north polar region, where the cold temperature in the lower troposphere necessitates a higher rate of decrease in refractivity and pressure with altitude. The vertical profile of temperature $T(h)$ that is obtained after the model-dependent ionospheric correction from the phase delay Φ_1 is shown in Fig. 9 (right panel). The changes of temperature $T(h)$ are concentrated in the 216- to 228-K interval when the altitude is increasing from 10 to 40 km (Fig. 9, right panel). The influence of tropopause, where the vertical gradient of temperature changes from -5 to $+2$ K/km, is evident in the 8- to 11-km altitude interval. The 11-K temperature increase with vertical gradient 0.9 K/km is visible in the 28- to 40-km altitude interval. The results of RO temperature measurements can be compared with the data of National Centers for Environmental Prediction (NCEP) analysis in this region that are relevant to the time of RO measurements.

The results of NCEP analysis have been obtained from the Web site http://www.cdc.noaa.gov/Composites/hour/ and are shown by open circles (Fig. 9, right panel) at the altitudes that correspond to pressure values 250, 200, 150, 100, 70, 50, 30, 20, and 10 hPa. Comparison of the results of RO data analysis with NCEP data indicates an accuracy of about ± 0.5 K in the 12- to 20-km height interval and $\sim \pm 1$–± 2 K at the 20- to 35-km altitudes. This indicates that the quality of the FORMOSAT-3/COSMIC RO measurements corresponds to that one observed in CHAMP experiments. The influence of the internal wave structures with amplitudes of about 1–3 K and vertical wavelength 1–3 km is clearly seen in the 11- to 28-km height interval.

The temperature vertical profiles in two equatorial and two moderate-latitude areas are shown in Figs. 10 and 11. The geographical coordinates of equatorial areas are 11.5° S, 63.8° W and 23.2° S, 59.0° W and are shown in Fig. 10 (left and right panels, respectively). These RO events are located in the equatorial and tropical parts of South America, respectively. The moderate-latitude RO events are located in the southern part of the Indian Ocean (with geographical coordinates 57.5° S and 295.1° W) and in the northern part of the Pacific Ocean (with geographical coordinates 55.5° N and 194.6° W), respectively (Fig. 11). The results of the NCEP analysis are shown by open circles (Figs. 10 and 11, right and left panels) at the altitudes that correspond to pressure values 200, 150, 100, 70, 50, 30, 20, and 10 hPa. The forms of the vertical temperature profiles are very different. In the equatorial and tropical regions of North America, the tropopause is clearly seen in the temperature profile with minimal temperatures ~190–196 K concentrated near the 17-km altitude. Above the tropopause, the temperature is increasing from 190 to 196 K (Fig. 10, left and right panels) at ~17 km up to 270–275 K at 46-km altitude (Fig. 10, left panel) and to 235–240 K at 37-km altitude (Fig. 10, right panel). Temperature variations observed in the 17- to 40-km height interval may be connected with influence of the internal atmospheric waves. Above the 36-km altitude (Fig. 10, left panel) and the 32-km altitude (Fig. 10, right panel), the temperature achieved maximal values of ~270 and 240 K, respectively. These maxima can correspond to the warming effect of the stratospheric ozone. Random temperature variations in the 36- to 46-km altitude interval are mainly caused by the high-frequency receiver noise. In the moderate-latitude area, one can see the multiple tropopause phenomena (Fig. 11). The first temperature minimum is located near the 10-km altitude. The minimal temperatures are also seen in the 10- to 22- and 10- to 28-km height intervals (Fig. 11, right and left panels, respectively). Small temperature variations in the 10- to 28-km height interval are connected with influence of the internal waves having the vertical wavelength 1–4 km. The temperature increases by 30–40 K at the altitudes 22–40 km up to the maximal value ~250–255 K at the 36- and 40-km height (Fig. 11, right and left panels). The statistical error in the temperature measurement is rapidly increasing and is about ± 4 K at the altitude 40–46 km (Fig. 11). Comparison of the results of RO data analysis with the NCEP data indicates good quality of the FORMOSAT-3/COSMIC RO measurements (Figs. 10 and 11).

Therefore, the results shown in Figs. 9–11 indicate a sufficient level of the accuracy of the temperature vertical profiles (± 0.5–± 2 K), which are found from the FORMOSAT-3/COSMIC RO frequency Φ_1 data, and reveal advantages of the application of the RO method to study meteorological parameters at different altitudes in the stratosphere and the upper troposphere.

V. Amplitude and Phase of the RO Signal as Radio Holograms of Internal Waves in the Atmosphere

The RO method is a new tool for studying the internal GWs on a global scale. Analysis of the temperature variations that were found from the RO phase data furnishes an opportunity to measure the statistical characteristics of the GW in the atmosphere as shown by [20], [26], and [27]. Global morphology of the GW activity in the stratosphere has been investigated in [20]. A vertical wavenumber spectrum of the normalized temperature fluctuations has been determined from the phase data of GPS/MET RO events in June/July 1995, October 1995, and February 1997, and the seasonal and latitudinal variations of the potential energy of the GW per unit mass have been estimated in [27].

The amplitude channels of the RO signal offer a new capability for investigating internal atmospheric waves [24], [33], [34], [42], [44], [49]. Quasi-regular structures are often seen in the amplitude data at heights that correspond to the tropopause and the lower stratosphere. These structures have the vertical wavelength in the range of 0.8–4 km and can be associated with GW transmitting energy and momentum through the troposphere to the stratosphere [26], [27], [30].

The goals of this section are 1) to compare the quality of the phase and amplitude channels of the RO radio holograms as a tool for observing the atmospheric internal waves and 2) to define the horizontal wind perturbations associated with GW by use of amplitude and phase of the RO signal.

Wave structures, as seen in the altitude dependences of the refraction attenuations X_p and X_a that are calculated from the phase acceleration (curve 1) and amplitude (curve 2) data [(13) and (16)], are shown in Fig. 12(a)–(d). The data in Fig. 12 correspond to four FORMOSAT-3 RO events: 0081—April 29, 48.0° N, 107.8° W (panel a); 0052—April 25, 1.6° N, 330.6° W (panel b), April 25, 35.0° S, 324.4° W (panel c), and April 25, 31.3° N, 198.5° W (panel d). For the calculation of the refraction attenuation from the phase excess data, the coefficient m in (6) has been evaluated using the satellites orbital data, which include the position and velocities of the GPS and LEO satellites relative to the center of the spherical symmetry point O (Fig. 6). The significant correspondence between the refraction attenuations that are obtained from the phase and amplitude data is clearly seen in Fig. 12(a)–(d) (curves 1 and 2). This correspondence is excellent when one considers the slow trend that describes the decrease of the refraction attenuation with height [Fig. 12(a)–(d)]. The high-frequency oscillations in the refraction attenuations that are found from the amplitude and phase data quantitatively coincide (Fig. 12, left and right panels). The small discrepancies in high-frequency oscillations (Fig. 12) may be connected with the

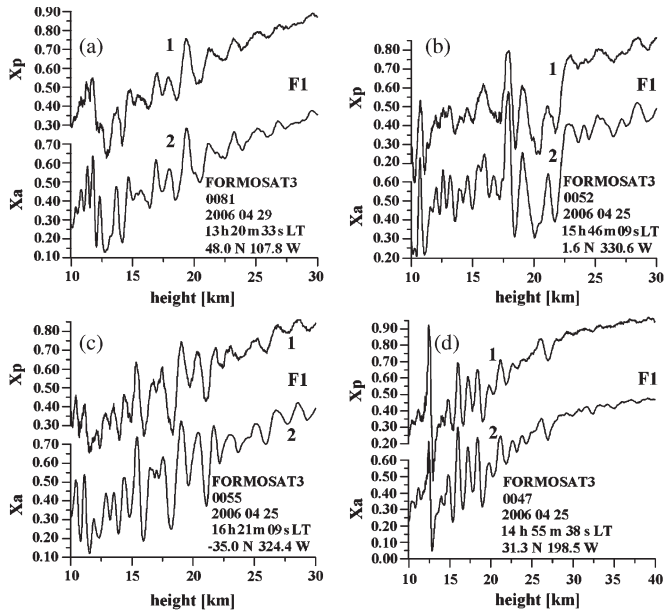

Fig. 12. Comparison of the refraction attenuations X_a and X_p calculated from the phase and amplitude data at the first GPS frequency f_1. Data shown in panels (a)–(d) correspond to four FORMOSAT-3 RO events: [panel (a)—April 29, 48.0° N, 107.8° W; panel (b)—April 25, 1.6° N, 330.6° W; panel (c)—April 25, 35.0° S, 324.4° W; and panel (d)—April 25, 31.3° N, 198.5° W].

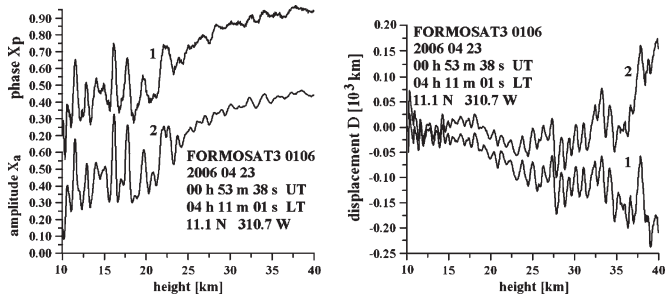

Fig. 13. (Left panel) Comparison of the refraction attenuations X_a and X_p calculated from the phase (curve 1) and amplitude (curve 2) data. (Right panel) Displacement D of the tangent point T calculated by use of (19) and (20) (curves 1 and 2, respectively).

influence of the diffraction effects, irregularities, and turbulence in the propagation medium and thermal noise. One can try to determine the displacement D of the tangent point T by use of the method described in Section II. An example of determination of the displacement D is shown in Fig. 13. The data shown in Fig. 13 correspond to the FORMOSAT-3 RO event 0106, April 23, 2006, 04 h 11 min 01 s LT, with geographical coordinates 11.1° N, 310.7° W. Curves 1 and 2 in Fig. 13 (left panel) demonstrate the significant correspondence between the refraction attenuations X_p and X_a evaluated from the phase acceleration and amplitude data [(15) and (18), respectively] at the first GPS frequency f_1. This correspondence allows one to determine the horizontal displacement D of the tangent point T. The results of the evaluation of the displacement D by use of (21)–(23) are shown in Fig. 13 (right panel). Curves 1 and 2 correspond to the values D that were found by use of the relationships (21), (23) and (22), (23), respectively. According to Fig. 13 (right panel), the displacement D estimated from

(22) and (23) is bounded between ± 25 km in the 10- to 16-km altitude interval and between ± 50 km in the 16- to 35-km height interval. This experimental result supports the theoretical estimations of the position of the tangent point in the atmosphere, which has been previously made [50], and opens a possibility to apply the method suggested in Section II for the location of the layered structures in the atmosphere and estimating their inclination. Earlier, this method has been successfully applied for the location of the inclined layered structures in the lower ionosphere [38] with the accuracy of about ± 150 km, which seems to be sufficient for determining the position of plasma layers in trans-ionospheric satellite–satellite links.

As observed from the analysis of the data shown in Figs. 12 and 13, relationship (15) is valid in the RO experiments up to altitudes of about 30–40 km. Relationship (15) opens a new way to measure the refraction attenuation in different kinds of RO experiments, which include the investigation of the planetary atmospheres. Thus, the phase acceleration has the same importance for the RO experiments as the well-known Doppler frequency. Note that by use of the phase data, one can correct the amplitude data for systematic errors that are caused by the trends in the antenna gain and direction and the receiver's noise variations. The interesting feature of the phase acceleration consists in the decrease of the ionospheric influence. The slow ionospheric trend, which is clearly seen in Fig. 8 (left panel, curves 1 and 2), introduces a systematic error in the phase path excesses at frequencies f_1 and f_2. This error is more than the contribution of the neutral component in the upper stratosphere. However, the slow ionospheric trend is not seen in the refraction attenuation [Figs. 12(a)–(d) and 13, left panel] because of the effect of double differentiation on time. Detailed validation of the suggested method for the location of the wave structures in the atmosphere is a task for future research.

The amplitudes of the refraction attenuation variations in Figs. 12 and 13 are decreasing with the increase of the altitude, thus indicating the atmospheric origin of the wave structures. The vertical wavelength of the wave structures is changing in the 1- to 4-km interval (Figs. 12 and 13) that is typical for atmospheric internal GWs [26], [27].

The polarization and dispersion GW relationships can be used to find the horizontal wind perturbations and kinetic energy of GW as formerly shown in [28]. The reply of GW can be obtained after subtracting the regular contribution from the refraction attenuations X_a and X_p. Curves 1 and 2 in Fig. 14 (left panel) demonstrate the refraction attenuations X_p and X_a evaluated from the phase acceleration and amplitude data [(15) and (18), respectively] for the FORMOSAT-3/COSMIC RO event 0003 (April 22, 2006, 17 h 33 min 40 s LT, geographical coordinates 74.3° N, 333.2° W) at the first GPS frequency f_1. Smooth curve 3 describes the results of modeling of the refraction attenuation. The significant correspondence between the refraction attenuations obtained from the amplitude and phase data is clearly seen in Fig. 14 (left panel; curves 1 and 2). This correspondence is excellent when one considers the slow trend that describes the decrease of the refraction attenuation with height (Fig. 14, left panel). The high-frequency oscillations in the refraction attenuations found from the amplitude and phase

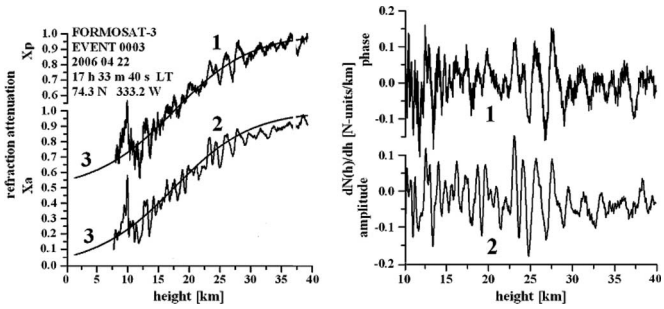

Fig. 14. (Left panel) The refraction attenuations X_a and X_p retrieved from the phase and amplitude data (curves 1 and 2, respectively). Curve 3 indicates the results of simulation of the refraction attenuation in the atmosphere. (Right panel) The variations of the vertical gradient of refractivity retrieved from the phase and amplitude data (curves 1 and 2, respectively).

data quantitatively coincide (Fig. 14, left and right panels). The results of modeling of the refraction attenuation coincide well with experimental data.

Previously, [24] and [42] showed that the amplitude variations of the RO signal can be used to find the vertical gradient of the refractivity $dN(h)/dh$. Equation (15) opens a new way to find the vertical gradient of refractivity by the same way as formerly used for the amplitude data [24]. The variations of the vertical gradient of refractivity $dN_p(h)/dh$ and $dN_a(h)/dh$ (N units/km) found from the FORMOSAT-3/COSMIC RO phase and amplitude data are compared in Fig. 14 (right panel; curves 1 and 2, respectively). There is a good correlation between $dN_p(h)/dh$ and $dN_a(h)/dh$ up to an altitude of 28 km (Fig. 14, right panel). Typical values of the vertical gradient variations are about ± 0.12–0.18 N units/km, and the typical vertical wavelength is 0.8–2.5 km. Changes in the vertical gradients of the refractivity may be connected with the GW that propagates through the tropopause areas and, consequently, may correspond to the changes in the horizontal wind velocity. At the 28- to 40-km altitudes, the amplitude and the form of wave structure are sharply changed. This indicates the wave-breaking zone in the 28- to 30-km interval. Note that an existence of the wave-breaking zone at 28–30 km at polar latitudes has been predicted earlier in some publications [51]. The amplitude of wave structure that decreased by two to three times corresponds to an energy dissipation of four to nine times. The wave-breaking effect and the instantaneous radio image of wave-breaking area are obtained by the FORMOSAT-3/COSMIC mission during the first time in the RO practice simultaneously in the amplitude and phase data. This observation supported the preliminary conclusion, which was made earlier in [24], on the possibility of studying the wave-breaking areas in the atmosphere using the amplitude RO method.

If the observed wave structures are caused by the GW activity, then the vertical gradients of refractivity can be related with horizontal wind perturbations by use of the GW polarization equations [24], [28].

The vertical profiles of the horizontal wind perturbations evaluated from the variations of the vertical gradient of refractivity by use of the method described in [28] are demonstrated in Fig. 15 (left panel). Curves 1 and 2 (Fig. 15, left panel) relate to the vertical profiles of the horizontal wind perturbations found from the phase and amplitude data and correspond to

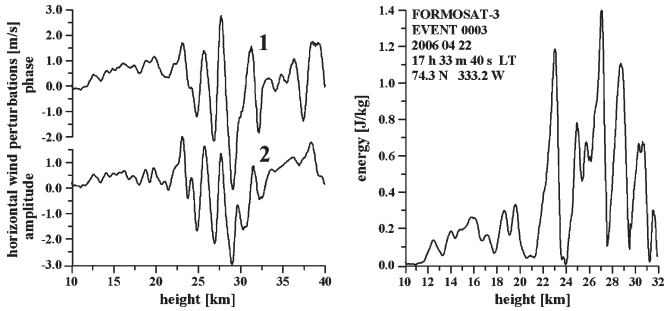

Fig. 15. (Left panel) The vertical profiles of the horizontal wind perturbations found from the phase and amplitude data (curves 1 and 2, respectively). (Right panel) Sum of the kinetic and potential energy of the wave structure.

the vertical gradient of refractivity shown by curves 1 and 2 in Fig. 14 (right panel). The horizontal wind perturbations are in the interval $\pm$2–3 m/s for both data found from the amplitude and the phase. The horizontal wind perturbations v can be recalculated to the kinetic energy of GW E_κ by means of the relation [27]

$$E_k = v^2/2 \text{ (J/kg)}. \tag{25}$$

The potential energy of GW can be found from the relationship [27]

$$E_p = g^2(\Delta T)^2 / \left(2T^2\omega_b^2\right) = g^2(\Delta N)^2 / \left(2N^2\omega_b^2\right) \text{ (J/kg)} \tag{26}$$

where g is the gravity acceleration (m/s^2), ω_b is the Brunt Vaisala frequency (1/s), ΔT and ΔN are the variations of temperature and refractivity in the GW, respectively, and $T(h)$ and $N(h)$ are the background vertical profiles of temperature and refractivity, respectively. The energy of GW E is the sum of the kinetic and potential energies, i.e.,

$$E = E_p(E_k = g^2 / \left(2\omega_b^2\right) (\Delta N)^2/N^2 + v^2/2 \text{ (J/kg)}. \tag{27}$$

The variations of refractivity ΔN can be found by integration from its vertical gradient (curves 1 and 2 in Fig. 15, right panel). The background vertical profile of the refractivity is shown in Fig. 8 (left panel). The result of evaluation of the GW energy is shown in Fig. 15 (right panel). The main part of the GW energy is concentrated in the 22- to 32-km altitude interval. Therefore, in this region, there is an active process of energy and kinetic moment transmission between different layers in the stratosphere. Note that the introduced interpretation of the GPS signal oscillations by GWs has been formerly checked [28] by comparing with the radiosondes measurements. More extensive validation study will be provided in future publications.

VI. Conclusion

The preliminary results of the FORMOSAT-3/COSMIC mission indicate new directions of application and necessitate the modernization of the RO method. A perspective direction for modernizing the RO method is connected with a new method of analysis of amplitude and phase variations in the RO signal. It is shown in this paper that the amplitude and phase variations of the RO signal contain important information on the vertical structure of the upper troposphere and the lower stratosphere. This information is primarily useful for studying quasi-periodical internal waves that propagate through the tropopause to stratosphere and is capable of characterizing GW in the 5- to 100-km range. The phase acceleration allows recalculating the phase delay to the refraction attenuation, which is important for the future RO mission aimed to measure the absorption in the atmosphere that is caused by water vapor and minor gas constituents. The phase acceleration and amplitude of the RO signal are important sources of information on the wave structures and give the radio image of the internal wave in the atmosphere. The wave-breaking effect and the instantaneous radio image of wave-breaking area are obtained by the FORMOSAT-3/COSMIC mission during the first time in the RO practice. This experimental information is important for the atmospheric science for comparing the results of theoretical modeling with actual atmospheric conditions. The application of this and other new techniques will generate extensive information on the internal wave properties in their propagation region.

Acknowledgment

The authors would like to thank the National Space Organization of Taiwan for the access of the FORMOSAT RO data.

References

[1] G. Fjeldbo and V. R. Eshleman, "The bistatic radar-occultation method for the study of planetary atmospheres," *J. Geophys. Res.*, vol. 70, pp. 3217–3225, 1965.

[2] O. I. Yakovlev, *Space Radio Science*. London, U.K.: Taylor & Francis. 2002, 320 p.

[3] T. P. Yunck, G. F. Lindal, and C. H. Liu, "The role of GPS in precise Earth observation," in *Proc. IEEE Position, Location and Navigat. Symp.*, Orlando, FL, Nov. 29–Dec. 2, 1988, pp. 251–258.

[4] A. S. Gurvich and T. G. Krasil'nikova, "Navigation satellites for radio sensing of the Earth's atmosphere," *Sov. J. Remote Sens.*, vol. 7, no. 6, pp. 1124–1131, 1990.

[5] C. Rocken, R. Anthes, M. Exner, D. Hunt, S. Sokolovskiy, R. Ware, M. Gorbunov, W. Schreiner, D. Feng, B. Herman, Y.-H. Kuo, and X. Zou, "Analysis and validation of GPS/MET data in the neutral atmosphere," *J. Geophys. Res.*, vol. 102, no. D25, pp. 29 849–29 866, 1997.

[6] E. R. Kursinski, G. A. Hajj, J. T. Schofield, R. P. Linfield, and K. R. Hardy, "Observing the Earth's atmosphere with radio occultation measurements using the global positioning system," *J. Geophys. Res.*, vol. 102, no. D19, pp. 23 429–23 465, 1997.

[7] R. Ware, M. Exner, D. Feng, M. Gorbunov, K. Hardy, B. Herman, Y. Kuo, T. Meehan, W. Melbourne, C. Rocken, W. Schreiner, S. Sokolovskiy, F. Solhelim, X. Zou, R. Anthes, S. Businger, and K. Trenberth, "GPS sounding of the atmosphere from low Earth orbit: Preliminary results," *Bull. Amer. Meteorol. Soc.*, vol. 77, no. 1, pp. 19–40, Jan. 1996.

[8] S. S. Leroy, "Measurement of geopotential heights by GPS radio occultation," *J. Geophys. Res.*, vol. 102, no. D6, pp. 6971–6986, 1997.

[9] A. Rius, G. Ruffini, and A. Romeo, "Analysis of ionospheric electron-density distribution from GPS/MET occultations," *IEEE Trans. Geosci. Remote Sens.*, vol. 36, no. 2, pp. 383–394, Mar. 1998.

[10] R. A. Anthes, C. Rocken, and Y. Kuo, "Applications of COSMIC to meteorology and climate," *Terr. Atmos. Ocean. Sci.*, vol. 11, no. 1, pp. 115–156, 2000.

[11] J. L. Garrison, A. Komjathy, V. U. Zavorotny, and S. J. Katzberg, "Wind speed measurement using forward scattered GPS signals," *IEEE Trans. Geosci. Remote Sens.*, vol. 40, no. 1, pp. 50–65, Jan. 2002.

[12] T. Elfouhaily, D. R. Thompson, and L. Linstrom, "Delay-Doppler analysis of bistatically reflected signals from the ocean surface: Theory and application," *IEEE Trans. Geosci. Remote Sens.*, vol. 40, no. 3, pp. 560–573, Mar. 2002.

[13] S. Mostert and J. A. Koekemoer, "The science and engineering payloads and experiments on SUNSAT," *Acta Astron.*, vol. 41, no. 4–10, pp. 401–411, 1997.

[14] A. Escudero, A. C. Schlesier, A. Rius, A. Flores, F. Rubek, G. B. Larsen, S. Syndergaard, and P. Hoeg, "Ionospheric tomography using Ørsted GPS measurements—Preliminary results," *Phys. Chem. Earth A*, vol. 26, no. 3, pp. 173–176, 2001.

[15] E. R. Kursinski and G. A. Hajj, "A comparison of water vapor derived from GPS occultations and global weather analyses," *J. Geophys. Res.*, vol. 106, no. D1, pp. 1113–1138, 2001.

[16] C. Reigber, H. Lühr, and P. Schwintzer, "CHAMP mission status," *Adv. Space Res.*, vol. 30, no. 2, pp. 129–134, Jul. 2002.

[17] G. A. Hajj, C. O. Ao, B. A. Iijima, D. Kuang, E. R. Kursinski, A. J. Mannucci, T. K. Meehan, L. J. Romans, M. de la Torre Juárez, and T. P. Yunck, "CHAMP and SAC-C atmospheric occultation results and intercomparisons," *J. Geophys. Res.*, vol. 109, no. D6, D06109, 2004. DOI: 10.129/2003JD003909.

[18] Y.-H. Kuo, T.-K. Wee, S. Sokolovskiy, C. Rocken, W. Schreiner, D. Hunt, and A. Anthes, "Inversion and error estimation of GPS radio occultation data," *J. Meteorol. Soc. Jpn.*, vol. 82, no. 1B, pp. 507–531, 2004.

[19] J. Wickert, T. Schmidt, G. Beyerle, G. Michalak, R. König, S. Heise, and C. Reigber, *GPS Radio Occultation With CHAMP and GRACE: Recent Results in Atmosphere and Climate Studies by Occultation Methods*, U. Foelsche, G. Kirchengast, and A. K. Steiner, Eds. New York: Springer-Verlag, 2006, pp. 3–16.

[20] T. Tsuda, M. Nishida, C. Rocken, and R. H. Ware, "A global morphology of GW activity in the stratosphere revealed by the GPS occultation data (GPS/MET)," *J. Geophys. Res.*, vol. 105, pp. 7257–7273, 2000.

[21] S. S. Leroy and G. R. North, "The application of COSMIC data to global change research," *Terr. Atmos. Ocean. Sci.*, vol. 11, no. 1, pp. 235–272, 2000.

[22] G. A. Hajj, E. R. Kursinski, L. J. Romans, W. I. Bertiger, and S. S. Leroy, "Technical description of atmospheric sounding by GPS occultation," *J. Atmos. Sol.-Terr. Phys.*, vol. 64, no. 4, pp. 451–469, 2002.

[23] A. Gobiet and G. Kirchengast, "Advancements of global navigation satellite system radio occultation retrieval in the upper stratosphere for optimal climate monitoring utility," *J. Geophys. Res.*, vol. 109, no. D24110, pp. 1–11, 2004. DOI:10.1029/2004JD005117.

[24] Y. A. Liou, A. G. Pavelyev, J. Wickert, S. F. Liu, A. A. Pavelyev, T. Schmidt, and K. Igarashi, "Application of GPS radio occultation method for observation of the internal waves in the atmosphere," *J. Geophys. Res.*, vol. 111, no. D06104, pp. 1–14, 2006. DOI:10.1029/2005JD005823.

[25] L. Froidevaux *et al.*, "Early validation analyses of atmospheric profiles from EOS MLS on the Aura satellite," *IEEE Trans. Geosci. Remote Sens.*, vol. 44, no. 5, pp. 1106–1121, May 2006.

[26] A. K. Steiner and G. Kirchengast, "GW spectra from GPS/MET occultation observations," *J. Atmos. Ocean. Technol.*, vol. 17, no. 4, pp. 495–503, Apr. 2000.

[27] T. Tsuda and K. Hocke, "Vertical wave number spectrum of temperature fluctuations in the stratosphere using GPS occultation data," *J. Meteorol. Soc. Jpn.*, vol. 80, no. 4B, pp. 1–13, 2002.

[28] Y. A. Liou, A. G. Pavelyev, C. Y. Huang, K. Igarashi, K. Hocke, and S. K. Yan, "Analytic method for observation of the gravity waves using radio occultation data," *Geophys. Res. Lett.*, vol. 30, no. 20, pp. ASC-1–ASC-5, 2003.

[29] Y. A. Liou, A. G. Pavelyev, J. Wickert, C. Y. Huang, S. K. Yan, and S. F. Liu, "Response of GPS occultation signals to atmospheric gravity waves and retrieval of gravity wave parameters," *GPS Solut.*, vol. 8, no. 2, pp. 103–111, Jul. 2004.

[30] T. Tsuda, M. V. Ratnam, P. T. May, M. J. Alexander, R. A. Vincent, and A. MacKinnon, "Characteristics of gravity waves with short vertical wavelengths observed with radiosonde and GPS occultation during DAWEX (Darwin Area Wave Experiment)," *J. Geophys. Res.*, vol. 109, no. D20, D20S03, 2004. DOI:10.1029/2004JD004946.

[31] A. G. Pavelyev, J. Wickert, Y. A. Liou, A. A. Pavelyev, and J. Jacobi, "Analysis of atmospheric and ionospheric wave structures using the CHAMP and GPS/MET radio occultation database," in *Atmosphere and Climate Studies by Occultation Methods*, U. Foelsche, G. Kirchengast, and A. Steiner, Eds. New York: Springer-Verlag, 2006, pp. 225–242.

[32] S. Sokolovskiy, "Inversion of radio occultation amplitude data," *Radio Sci.*, vol. 35, no. 1, pp. 97–105, 2000.

[33] K. Igarashi, A. G. Pavelyev, K. Hocke, D. A. Pavelyev, I. A. Kucherjavenkov, S. S. Matugov, A. I. Zakharov, and O. I. Yakovlev, "Radio holographic principle for observing natural processes in the atmosphere and retrieving meteorological parameters from radio occultation data," *Earth Planets Space*, vol. 52, no. 11, pp. 893–899, 2000.

[34] A. Pavelyev, K. Igarashi, C. Reigber, K. Hocke, J. Wickert, G. Beyerle, S. Matyugov, A. Kucherjavenkov, D. Pavelyev, and O. Yakovlev, "First application of radioholographic method to wave observations in the upper atmosphere," *Radio Sci.*, vol. 37, no. 3, pp. 15-1–15-11, 2002.

[35] S. Sokolovskiy, W. Schreiner, C. Rocken, and D. Hunt, "Detection of high-altitude ionospheric irregularities with GPS/MET," *Geophys. Res. Lett.*, vol. 29, no. 3, pp. 1033–1037, 2002. DOI:10.1029/2001GL013398.

[36] M. E. Gorbunov, A. S. Gurvich, and A. V. Shmakov, "Back-propagation and radio-holographic methods for investigation of sporadic ionospheric E-layers from Microlab-1 data," *Int. J. Remote Sens.*, vol. 23, no. 4, pp. 675–685, Feb. 2002.

[37] J. Wickert, A. G. Pavelyev, Y. A. Liou, T. Schmidt, C. Reigber, K. Igarashi, A. A. Pavelyev, and S. Matyugov, "Amplitude variations in GPS signals as a possible indicator of ionospheric structures," *Geophys. Res. Lett.*, vol. 31, no. 24, pp. L24 801.1–L24 801.4, 2004. DOI:10.1029/2004GL020607.

[38] Y. A. Liou and A. G. Pavelyev, "Simultaneous observations of radio wave phase and intensity variations for locating the plasma layers in the ionosphere," *Geophys. Res. Lett.*, vol. 33, no. 23, pp. L23 102.1–L23 102.5, 2006. DOI:10.1029/2006GL027112.

[39] K. Hocke, A. Pavelyev, O. Yakovlev, L. Barthes, and N. Jakowski, "Radio occultation data analysis by radio holographic method," *J. Atmos. Sol.-Terr. Phys.*, vol. 61, no. 15, pp. 1169–1177, 1999.

[40] A. K. Steiner, G. Kirchengast, and H. P. Ladreiter, "Inversion, error analysis and validation of GPS/MET data," *Ann. Geophys.*, vol. 17, no. 1, pp. 122–138, 1999.

[41] A. G. Pavelyev, T. Tsuda, K. Igarashi, Y. A. Liou, and K. Hocke, "Wave structures in the electron density profile in the ionospheric D and E-layers observed by radio holography analysis of the GPS/MET radio occultation data," *J. Atmos. Sol.-Terr. Phys.*, vol. 65, no. 1, pp. 59–70, 2003.

[42] Y. A. Liou, A. G. Pavelyev, C. Y. Huang, K. Igarashi, and K. Hocke, "Simultaneous observation of the vertical gradients of refractivity in the atmosphere and electron density in the lower ionosphere by radio occultation amplitude method," *Geophys. Res. Lett.*, vol. 29, no. 19, pp. 43-1–43-4, 2002.

[43] A. Pavelyev, A. V. Volkov, A. I. Zakharov, S. A. Krytikh, and A. I. Kucherjavenkov, "Bistatic radar as a tool for Earth investigation using small satellite," *Acta Astron.*, vol. 39, no. 9, pp. 721–730, 1996.

[44] A. G. Pavelyev, Y. A. Liou, and J. Wickert, "Diffractive vector and scalar integrals for bistatic radio holographic remote sensing," *Radio Sci.*, vol. 39, no. 4, pp. RS4011.1–RS4011.16, 2004. DOI:10.1029/2003RS002935.

[45] E. Martini, A. Freni, L. Facheris, and F. Cuccoli, "Impact of tropospheric scintillation in the Ku/K bands on the communications between two LEO satellites in a radio occultation geometry," *IEEE Trans. Geosci. Remote Sens.*, vol. 44, no. 8, pp. 2063–2071, Aug. 2006.

[46] S. Sokolovskiy, C. Rocken, D. Hunt, W. Schreiner, J. Johnson, D. Masters, and S. Esterhuizen, "GPS profiling of the lower troposphere from space: Inversion and demodulation of the open-loop radio occultation signals," *Geophys. Res. Lett.*, vol. 33, no. L14816, pp. 1–4, 2006. DOI:10.1029/2006GL026112.

[47] J. J. Spilker, "GPS signal structure and performance characteristics," in *Global Positioning System*, P. M. Janiczek, Ed. Washington, DC: Inst. Navig., 1980, pp. 29–54.

[48] V. V. Vorobev and T. G. Krasilnikova, "Estimation of accuracy of the atmosphere refractive index recovery from Doppler shift measurements at frequencies used in the NAVSTAR system," *Izv. Russian Acad. Sci., Phys. Atmos. Ocean. Engl. Transl.*, vol. 29, no. 7, pp. 602–609, 1994.

[49] K. Igarashi, A. Pavelyev, K. Hocke, D. Pavelyev, and J. Wickert, "Observation of wave structures in the upper atmosphere by means of radio holographic analysis of the radio occultation data," *Adv. Space Res.*, vol. 27, no. 6/7, pp. 1321–1327, 2001.

[50] S. Syndergaard, E. R. Kursinski, B. M. Herman, E. M. Lane, and D. E. Flittner, "A refractive index mapping operator for assimilation of occultation data," *Mon. Weather Rev.*, vol. 133, no. 9, pp. 3217–3242, 2005. DOI: 10.1175/MWR3001.1.

[51] Y. D. Afanasyev and W. R. Peltier, "Numerical simulation of internal gravity wave breaking in the middle atmosphere: The influence of dispersion and three-dimensionalization," *J. Atmos. Sci.*, vol. 58, no. 2, pp. 132–153, Jan. 2001.

Yuei-An Liou (S'91–M'96–SM'01) received the B.S. degree in electrical engineering (EE) from National Sun Yat-Sen University, Kaohsiung, Taiwan, R.O.C., in 1987 and the M.S.E. degree in EE, the M.S. degree in atmospheric and space sciences, and the Ph.D. degree in EE and atmospheric, oceanic, and space sciences from the University of Michigan, Ann Arbor, in 1992, 1994, and 1996, respectively.

From 1989 to 1990, he was a Research Assistant with the Robotics Laboratory, National Taiwan University. From 1991 to 1996, he was a Graduate Student Research Assistant with the Radiation Laboratory, University of Michigan, where he developed land–air interaction and microwave emission models for prairie grassland. He joined the faculty of the Center for Space and Remote Sensing Research (CSRSR) in 1996, Institute of Space Sciences in 1997, and Department of Electrical Engineering in 2005, all at the National Central University, Taoyuan, Taiwan, where he is now a Professor and the Director of the CSRSR. He served as the Division Director, Science Research Division, National Space Organization (NSPO), Taiwan, in 2005 and continued to serve as an Advisor to NSPO in 2006. In August 2006, he became a Chair Professor and the Dean of the College of Electrical Engineering and Computer Science, Ching Yun University, Jung Li, Taiwan. His current research activities include GPS meteorology and ionosphere, remote sensing of the atmosphere and land surface, land surface processes modeling, and application of neural networks and fuzzy systems in inversion problems. He is a Principal Investigator on many research projects sponsored by the National Science Council (NSC), Council of Agriculture, NSPO, Civil Aeronautics Administration, Minister of Interior, Water Conservancy Agency of Taiwan, and Office of Naval Research of USA. He has over 60 referral papers and more than 130 international conference papers. He is a referee for *Terrestrial, Atmospheric and Oceanic Sciences*, IEEE TRANSACTIONS ON GEOSCIENCE AND REMOTE SENSING (IEEE TGRS), *Asian Journal of Geoinformatics*, *International Journal of Remote Sensing*, *Earth, Planets and Space*; *Water Resources Research*; *Environmental Modelling and Software*; and *Remote Sensing of Environment*. He is a member of the Editorial Advisory Board to *GPS Solutions* and serves as a Guest Editor for the June 2005 Special Issue of "GPS Radio Occultation (RO) Experiments" of *GPS Solutions*.

Dr. Liou serves as a leading Guest Editor for the IEEE TGRS special issue "Meteorology, Climate, Ionosphere, Geodesy, and Reflections from the Ocean Surfaces: Studies by Radio Occultation Methods." He is listed in *Who's Who in the World*. He was a recipient of the Annual Research Awards from NSC in 1998, 1999, and 2000, a recipient of the First Class Research Awards from NSC in 2004, 2005, and 2006, and a recipient of the NCU Outstanding Research Awards in 2004 and 2006. He was awarded the "Contribution Award to FORMOSAT-3 National Space Mission" by NSPO in 2006. He is a member of the American Geophysical Union, the American Meteorological Society, and the International Association of Hydrological Sciences, and a Senior Member of the Institute of Electrical and Electronics Engineers, Inc. He is an Honorary Life Member of the Korean Society of Remote Sensing.

Alexander G. Pavelyev was born in 1938 in Russia. He received the B.S. and M.S. degrees from Gorky State University, Gorky, Russia, in 1961 and the Ph.D. degree in radio physics from the Academy of Sciences of the USSR, Moscow, Russia, in 1969.

He became a Senior Researcher (Assistant Professor) on February 6, 1977. Since June 2000, he has been the Head of the Laboratory of Radio Wave Propagation in Space of the Institute of Radio Engineering and Electronics, Russian Academy of Sciences, Moscow.

Shuo-Fang Liu received the B.S. and M.S.E. degrees from the National Cheng-Kung University, Tainan, Taiwan, R.O.C., in 1986 and 1993, respectively, and the Ph.D. degree from National Central University, Chung-Li, Taiwan, in 2002.

From 1993 to 2002, he was an Instructor of industrial design with the Oriental Institute of Technology, Baan-Chyau, Taipei, Taiwan. He is now an Assistant Professor with the Department of Industrial Design, National Cheng-Kung University. His current research activities include QFD and product design development, human–computer interface, augmented reality, and multimedia applications.

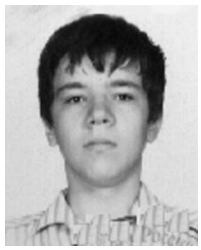

Alexey A. Pavelyev was born in Russia in 1986. He received the B.S. degree from the Remote Sensing Ecological Department of the Moscow Chemical Technology University, Moscow, Russia.

He is currently working as Junior Scientist in the Institute of Radio Engineering and Electronics, Russian Academy of Sciences, Moscow.

Nick Yen received the B.S. degree in engineering from Tsing Hua University, Hsinchu, Taiwan, R.O.C., in 1976 and the M.S. degree in mechanical engineering from Oregon State University, Corvallis, in 1980.

He started his career at Ford Aerospace Corporation in Palo Alto, CA, as an Antenna Design/Analysis Engineer between 1981 and 1984, after graduate school from Oregon State University. In 1985, he transferred to RCA Astro and continued to be an Antenna Engineer in East Windsor, NJ, for a year. In 1986, he returned to Ford Aerospace Corporation (later became Space System Loral) until 2003. From 1986 to 1992, he primarily continued as an Antenna Design Engineer and Antenna Project Manager. Between 1992 and 2003, he held many key positions in Space System Loral that include SUPERBIRD Senior System Engineer, MBSAT Antenna Subsystem Manger, Control Mechanisms Department Manager, Launch Integration and Launch Operation Department Manager, and Europe*Star Deputy Executive Director. He joined the National Space Organization (NSPO) in 2004 to begin his duty as the Deputy Program Director for the FORMOSAT-3/COSMIC Program, a Taiwan–U.S. joint science mission for the research and the application of the radio occultation technique. He successfully managed to complete the launch mission of a six-satellite constellation in April 2006. He is currently the FORMOSAT-3 Program Director that takes charge of the five-year mission plan, in addition to the current FORMOSAT-3/COSMIC constellation mission operation and the continuous program promotions to global users. He is currently working on the planning and the implementation of the follow-on FORMOSAT-3/COSMIC missions at NSPO.

C.-Y. Huang, photograph and biography not available at the time of publication.

Chen-Joe Fong (S'04) received the B.S.E.E. and M.S.E.E. degrees in electrophysics and electro-optical engineering from the National Chiao-Tung University (NCTU), Hsinchu, Taiwan, R.O.C., in 1983 and 1985, respectively, where he is currently working toward the Ph.D. degree.

He is a Research Fellow and the FORMOSAT-3 program Systems Engineering Manager of the National Space Organization (NSPO), National Applied Research Laboratory, Taiwan, R.O.C. During the FORMOSAT-3 constellation mission operation phase, he acted as a Spacecraft Lead and was responsible for the spacecraft anomaly resolution. He joined NSPO in 1993 and started as an Associate Researcher, Researcher, Electrical Development Model (EDM) Test Engineering Lead, Deputy Lead of the NSPO engineering team at TRW (NETT), and Satellite Test Manager, and later acted as Satellite Integration & Test (I&T) Project Manager of the ROCSAT-1 (later named FORMOSAT-1) program, Satellite Launch Conductor in the ROCSAT-1 launch campaign, and later an I&T Division Director in charge of the NSPO satellite I&T facility. Then, he joined the FORMOSAT-3 program and started as a Resident Team Manager at Orbital and System Engineering Lead. From 1987 to 1993, he was with the Center for Measurement Standards as an Associated Researcher, Researcher, Section Manager, and later a Microwave Lab Head, and was with the Center for Aviation and Space Technology of Industrial Technology Research Institute as a Systems Engineer for the ROCSAT-1 program. His current research interests include GPS radio occultation, remote sensing, systems engineering, mission simulation, polarization mode dispersion, incoherent time-domain pump fiber Raman amplifier, and optical solutions.

Mr. Fong is a member of the American Institute of Aeronautics and Astronautics and the Optical Society of America. He is a Permanent Member of the Aeronautical and Astronautical Society of the Republic of China and also a member of the Phi-Tau-Phi Scholastic Honor Society.